EARTHQUAKE ENGINEERING AND STRUCTURAL DYNAMICS, VOL. 26, 515–528 (1997)

DYNAMIC ANALYSIS OF BASE-ISOLATED SHEAR BEAMS BUMPING AGAINST STOPS

HSIANG-CHUAN TSAI*

Department of Construction Engineering, National Taiwan Institute of Technology, P.O. Box 90-130, 43, Section 4, Keelong Road, Taipei, Taiwan, R.O.C.

SUMMARY

Base isolation requires a gap between the base-isolated building and its surroundings to provide space for the deformation of isolation system. Bumping against the surroundings may change the performance of the base-isolated building. In this study, the building is modelled as an elastic or inelastic shear beam and the surroundings is simplified as elastic or inelastic stops. The influence of stop stiffness, gap size and stop strength on the seismic response is studied. Numerical results indicate that the impact wave induced by the bumping can create an extremely high acceleration response in the shear beam, if the shear beam remains elastic. A non-linearly elastic stop model is observed to reduce the acceleration response. If the shear beam yields, the impact wave cannot propagate through the shear beam and the shear beam remains in the low acceleration response except for the base. Changing the stop stiffness or stop strength has little effect on the distribution of ductility demand along the shear beam. © 1997 by John Wiley & Sons, Ltd.

KEY WORDS: base isolation; bumping; shear beam; dynamic analysis

1. INTRODUCTION

An isolation system applied in base-isolated buildings is generally capable of both flexibility and energy dissipation. Flexibility in the horizontal direction will lower the fundamental frequency of the building to below the range of frequencies which dominate general earthquake input so that the earthquake-induced acceleration will be decreased. The low stiffness of the isolation system could cause the displacement of the building relative to the ground to become unacceptably large. Consequently, the isolation system itself must have some energy-dissipating capacity to reduce the base displacement. Even though the isolation system can supply damping to the building, the base-isolated building still has a relatively large horizontal displacement during earthquakes. An isolation gap between the isolated building and its surroundings must be provided to permit for this displacement. Furthermore, special architectural details must be incorporated to prevent any undesirable interaction.

Theoretically, bumping of the base-isolated building against its surroundings will never occur, if the size of the isolation gap is designed according to 'extreme' earthquake motions. However, it is obvious that bumping against the surroundings can significantly change the performance of the base-isolated buildings. Understanding the characteristics of bumping of the base-isolated structures can be important in order to provide guidance in the design of the isolation gap and upper structure.

In the 1994 Northridge earthquake, several unusually high-frequency spikes were found in the accelerograms of a base-isolated building because architectural details have compromised the isolation gap and imparted an impulsive force to the building.[1] Although no upper structure damage resulted from these short-duration acceleration spikes, this event indicates that misuse of the isolation gap can affect the seismic response of base-isolated buildings, even if the intensity of earthquake is below the design level. However, very few of the

* Professor

CCC 0098–8847/97/050515–14$17·50

Received 19 August 1994
Revised 10 October 1996

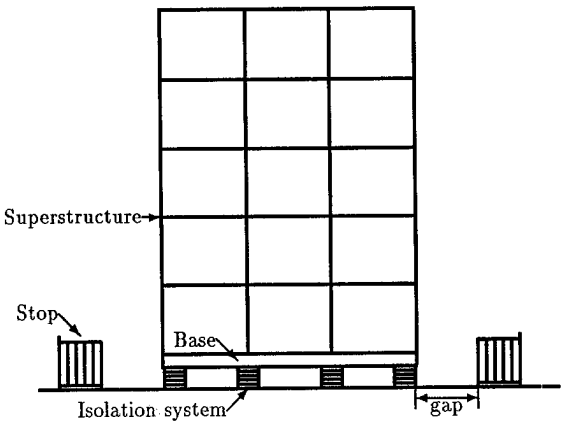

Figure 1. Base-isolated structure and isolation gap

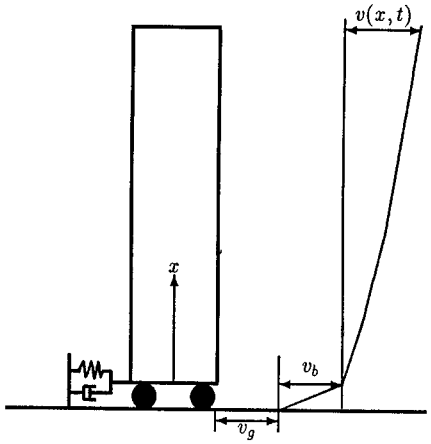

Figure 2. Base-isolated shear beam model

past research of base isolation has placed an emphasis on the influence of the surroundings on the response of base-isolated structures.[2]

In this study, the surroundings are simplified as stops with spring and dash-pot separated by gaps from the base of the building. The force–displacement relation of the stop is assumed as linearly elastic, non-linearly elastic or elastoplastic. The isolation system is modelled as either linearly elastic or bilinearly elastoplastic. At first, the superstructure is modelled as a viscoelastic shear beam and a non-linear equation of motion in terms of the base deformation and the mode amplitudes of the shear beam is derived. The dynamic behaviours of the elastic shear beam bumping against the different types of stops during earthquakes are studied. For extreme earthquake events, the response of the base-isolated buildings would be dominated by the inelastic response. The superstructure is then modelled as an elastoplastic shear beam and the non-linear finite element method is applied to study the inelastic response of the isolated shear beam bumping against the stops.

Under the excitation of 'extreme' earthquakes, the isolation system would reach its limit state[3] and the base-isolated building may remain in an unstable condition before bumping against the stops. Current practices in the design of base-isolated buildings allow for provision of a fail-safe mechanism, such as stub columns,[4] which eliminates the possibility of a base-isolated building remaining unstable during extreme ground motion. However, since the object of this paper is emphasized on the bumping, the isolation system is assumed here to be still in the stable condition and the fail-safe devices are assumed to be not activated.

2. BASE-ISOLATED SHEAR BEAM

A base-isolated building and its surrounded stops are shown in Figure 1. Since only horizontal degrees of freedom are considered, the superstructure can be modelled as a viscoelastic vertical shear beam of length l as shown in Figure 2. The shear beam has mass density ρ, cross-sectional area A, effective shear area A_s, shear modulus G and damping coefficient C. Both the isolation system and the stops apply the horizontal force to the base of the building. Consequently, their stiffness and damping are represented by a spring and a dash-pot connected to the base of the shear beam. The properties of the spring and dash-pot are not linear, depending on the type of the isolation system utilized and the model of the stops assumed.

The absolute transverse displacement of the base-isolated shear beam is

$$v_t(x,t) = v_g(t) + v_b(t) + v(x,t) \tag{1}$$

in which v_g is the ground displacement, v_b is the base displacement relative to the ground and $v(x,t)$ is the transverse displacement of the shear beam relative to the base. The equation of motion of the shear beam excited by ground acceleration $\ddot{v}_g(t)$ is

$$GA_s\frac{\partial^2 v}{\partial x^2}+CA_s\frac{\partial^3 v}{\partial x^2\partial t}-\rho A\frac{\partial^2 v}{\partial t^2}-\rho A\frac{\mathrm{d}^2 v_b}{\mathrm{d}t^2}=\rho A\ddot{v}_g \tag{2}$$

If the shear beam is linearly elastic, the displacement of the shear beam relative to the base can be expressed as the linear combination of the undamped fixed-base mode shapes, $\phi_i(x)$,

$$v(x,t)=\sum_{i=1}^{\infty}\phi_i(x)Y_i(t) \tag{3}$$

where Y_i is the amplitude of the ith fixed-base mode. The mode shape of the nth vibration mode for the fixed-base shear beam can be derived as

$$\phi_n(x)=\sin(n-\tfrac{1}{2})\pi\frac{x}{l} \tag{4}$$

The corresponding frequency is

$$\omega_n=\frac{(n-\frac{1}{2})\pi}{l}\sqrt{\frac{GA_s}{\rho A}} \tag{5}$$

According to the orthogonality properties of mode shapes, equation (2) can be reduced to the equations of motion in terms of the amplitude of each fixed-base mode:

$$M_n\ddot{Y}_n+2\xi_n\omega_n M_n\dot{Y}_n+\omega_n^2 M_n Y_n+P_n\ddot{v}_b=-P_n\ddot{v}_g \tag{6}$$

in which ξ_n is the damping ratio of the nth fixed-base mode, defined as

$$\xi_n=\frac{C}{2G}\omega_n \tag{7}$$

M_n is the modal mass defined as

$$M_n=\rho A\int_0^l\phi_n^2(x)\,\mathrm{d}x=\tfrac{1}{2}\rho Al \tag{8}$$

and P_n is defined as

$$P_n=\rho A\int_0^l\phi_n(x)\,\mathrm{d}x=\frac{\rho Al}{(n-\frac{1}{2})\pi} \tag{9}$$

If the spring is linear, the following equation is established by considering the force equilibrium of the whole model in Figure 2,

$$\rho A\int_0^l\frac{\partial^2 v}{\partial t^2}\,\mathrm{d}x+m\ddot{v}_b+c\dot{v}_b+kv_b=-m\ddot{v}_g \tag{10}$$

in which $m=\rho Al$ is the total mass of the shear beam, k is the stiffness of the spring and c is the damping coefficient of the dash-pot. Substituted by equation (3), the above equation becomes

$$\sum_{i=1}^{\infty}P_i\ddot{Y}_i+m\ddot{v}_b+c\dot{v}_b+kv_b=-m\ddot{v}_g \tag{11}$$

An equation in matrix form is established by combining equations (6) and (11), i.e.,

$$\begin{bmatrix} m & P_1 & P_2 & \cdots \\ P_1 & M_1 & 0 & \cdots \\ P_2 & 0 & M_2 & \cdots \\ \vdots & \vdots & \vdots & \ddots \end{bmatrix} \begin{Bmatrix} \ddot{v}_b \\ \ddot{Y}_1 \\ \ddot{Y}_2 \\ \vdots \end{Bmatrix} + \begin{bmatrix} c & 0 & 0 & \cdots \\ 0 & 2\xi_1\omega_1 M_1 & 0 & \cdots \\ 0 & 0 & 2\xi_2\omega_2 M_2 & \cdots \\ \vdots & \vdots & \vdots & \ddots \end{bmatrix} \begin{Bmatrix} \dot{v}_b \\ \dot{Y}_1 \\ \dot{Y}_2 \\ \vdots \end{Bmatrix}$$

$$+ \begin{bmatrix} k & 0 & 0 & \cdots \\ 0 & \omega_1^2 M_1 & 0 & \cdots \\ 0 & 0 & \omega_2^2 M_2 & \cdots \\ \vdots & \vdots & \vdots & \ddots \end{bmatrix} \begin{Bmatrix} v_b \\ Y_1 \\ Y_2 \\ \vdots \end{Bmatrix} = - \begin{Bmatrix} m \\ P_1 \\ P_2 \\ \vdots \end{Bmatrix} \ddot{v}_g \tag{12}$$

which can be simply expressed as

$$\mathbf{M}\ddot{\mathbf{y}} + \mathbf{C}\dot{\mathbf{y}} + \mathbf{K}\mathbf{y} = \mathbf{f} \tag{13}$$

3. SOLUTION SCHEME

Because the spring and dash-pot which represent the isolation system and stops are non-linear, equation (13) becomes a system of non-linear equations. To find the solution of the non-linear dynamic response, equation (13) must be revised to be in an incremental form; in addition, the spring constant k is replaced by the tangential stiffness $\partial(f_S + f_I)/\partial v_b$ where f_S is the spring force of stops and f_I is the spring force of isolators. The force–displacement relations of the stops and the isolators used in this paper are shown in Figures 3 and 4, respectively. Using the modified Newton–Raphson iteration scheme and the Newmark's implicit integration method,[5] the following governing equilibrium equation at the ith iteration of the nth time step is derived:

$$\left(\frac{1}{\Delta^2\beta}\mathbf{M} + \frac{\gamma}{\Delta\beta}\mathbf{C}_n^{(i)} + \mathbf{K}_n^{(i)}\right)\mathbf{q}_n^{(i)} = \mathbf{r}_n^{(i)} \tag{14}$$

in which β and γ are the parameters of the Newmark method and Δ is the time step. $\mathbf{C}_n^{(i)}$ and $\mathbf{K}_n^{(i)}$ represent the matrices $\mathbf{C}$ and $\mathbf{K}$ defined in equation (13) at the ith iteration of the nth time step. The vector $\mathbf{q}_n^{(i)}$ is the displacement increment from which the displacement vector $\mathbf{y}$ of the $(i+1)$th iteration can be found:

$$\mathbf{y}_n^{(i+1)} = \mathbf{y}_n^{(i)} + \mathbf{q}_n^{(i)} \tag{15}$$

The vector $\mathbf{r}_n^{(i)}$ is the residual vector of the ith iteration which equals to

$$\mathbf{r}_n^{(i)} = \mathbf{f}_n - \mathbf{g}_n^{(i)} \tag{16}$$

in which $\mathbf{f}_n$ is the vector $\mathbf{f}$ of the nth time step defined in equation (13) and $\mathbf{g}_n^{(i)}$ is the internal force vector at the ith iteration of the nth step.

According to the special forms of the matrices of $\mathbf{M}$, $\mathbf{C}$ and $\mathbf{K}$ defined in equation (12), equation (14) has the following matrix form:

$$\begin{bmatrix} \Lambda_b & \Lambda_{b1} & \Lambda_{b2} & \cdots & \Lambda_{bN} \\ \Lambda_{b1} & \Lambda_1 & 0 & \cdots & 0 \\ \Lambda_{b2} & 0 & \Lambda_2 & \cdots & 0 \\ \vdots & \vdots & \vdots & \ddots & \vdots \\ \Lambda_{bN} & 0 & 0 & \cdots & \Lambda_N \end{bmatrix} \begin{Bmatrix} q_b \\ q_1 \\ q_2 \\ \vdots \\ q_N \end{Bmatrix} = \begin{Bmatrix} r_b \\ r_1 \\ r_2 \\ \vdots \\ r_N \end{Bmatrix} \tag{17}$$

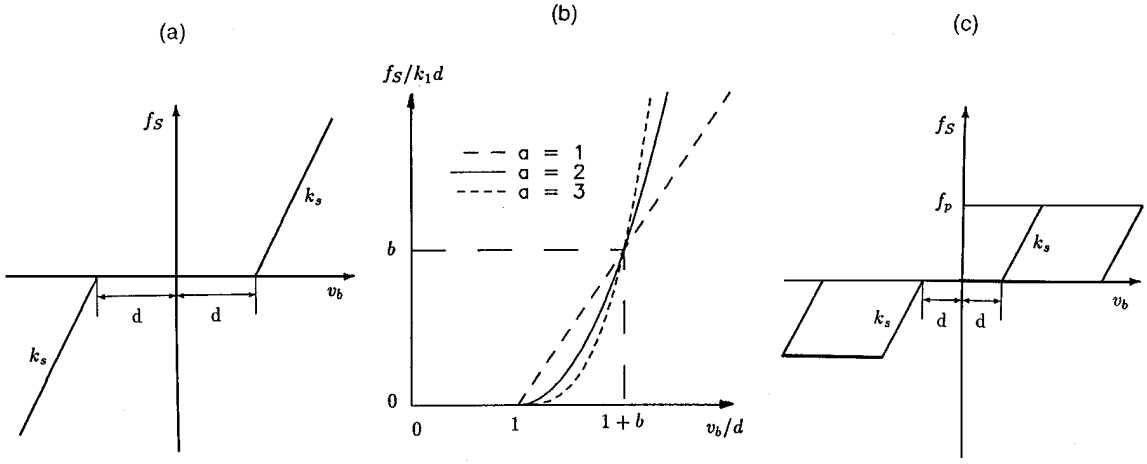

Figure 3. Force–displacement relations of stops: (a) linear elastic stop; (b) non-linear elastic stop; (c) inelastic stop

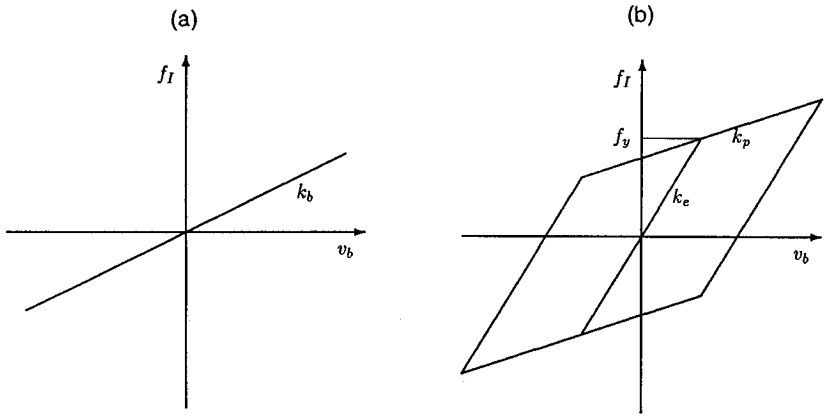

Figure 4. Force–dispalcement relations of isolators: (a) linear isolator; (b) bilinear isolator

in which N is the number of fixed-base shear beam modes used in calculation. The above equation indicates that

$$\Lambda_{\mathrm{b}} q_{\mathrm{b}} + \sum_{i=1}^{N} \Lambda_{\mathrm{bi}} q_i = r_{\mathrm{b}} \tag{18}$$

and

$$q_i = \frac{r_i - \Lambda_{\mathrm{bi}} q_{\mathrm{b}}}{\Lambda_i} \tag{19}$$

from which q_{b} is found

$$q_{\mathrm{b}} = \frac{r_{\mathrm{b}} - \sum_{i=1}^{N} \Lambda_{\mathrm{bi}} r_i / \Lambda_i}{\Lambda_{\mathrm{b}} - \sum_{i=1}^{N} \Lambda_{\mathrm{bi}}^2 / \Lambda_i} \tag{20}$$

The effort to compute the displacement increment of the iteration, q_b and q_i, from equations (20) and (19) is markedly less than the normal Gauss elimination.

4. RESPONSE FOR LINEARLY ELASTIC STOP

The force–displacement relation of a linearly elastic stop is shown in Figure 3(a) in which f_S is the spring force, d is the gap size and k_s is the stop stiffness. In the numerical study, a building is modelled as a shear beam of which the height is $l = 15$ m, the mass per unit length is $\rho A = 1400$ kg/m and the shear stiffness is $GA_s = 102 \cdot 06$ MN. The damping ratios of the shear beam defined in equation (7) are assumed to be independent of frequency and are equal to $\xi_n = 0 \cdot 014$. The frequencies of the first three modes for the fixed-base model are $4 \cdot 5, 13 \cdot 5$ and $22 \cdot 5$ Hz. The stiffness of the linear isolator defined in Figure 4(a) is $k_b = 210$ kN/m and the damping coefficient is $c_b = 6640$ N s/m. The natural frequency of the isolation system is $\omega_b = \sqrt{k_b/\rho Al} = 0 \cdot 503$ Hz and the damping ratio is $\xi_b = c_b/(2\omega_b \rho Al) = 0 \cdot 05$. The stiffness of linearly elastic stops is assumed to be $k_s = 210$ MN/m. The ratio of the stop stiffness to the isolator stiffness is $R_k = k_s/k_b = 1000$. The damping of the stops is neglected. The input ground acceleration is the 1940 El Centro earthquake record in which the peak acceleration is $0 \cdot 348$ g. Ten fixed-base modes are utilized in the analysis, the highest frequency of which is $85 \cdot 5$ Hz. The parameters of the Newmark method are $\beta = 0 \cdot 25$ and $\gamma = 0 \cdot 5$. The time step is $\Delta = 0 \cdot 001$ s.

The responses of the base-isolated shear beam are computed according to the aforementioned methodology. The variations of the maximum accelerations with the gape size at the base and top of the shear beam excited by the El Centro earthquake are plotted in Figure 5(a). Also shown in this figure is the peak time when the maximum base acceleration occurs, which indicates that bumping for various gap sizes can be grouped into two categories. For the gap smaller than 0·08 m, the peak time occurs after approximately two seconds. For the larger gap, the peak time changes to the sixth second. Two categories have the same variation pattern for the maximum acceleration. With an increasing gap size, the maximum response increases initially. After some gap size, however, the maximum response becomes to decrease. The magnitude of the maximum acceleration in the category of larger gap is smaller than that in the category of smaller gap.

The acceleration history at the base of the shear beam is plotted in Figure 5(b) for the gap equal to 0·10 m. Spikes of very high acceleration caused by the impact of the stops on the shear beam are observed. The displacement history at the base for 0·10 m gap is compared in Figure 6(a) with that without stops, indicating that four bumps occurred during the fifth and seventh seconds. The corresponding acceleration responses are plotted in Figure 6(b) in which the points whose acceleration is higher than 2 m/s^2 have been clipped. Figure 6 indicates that the linearly elastic stops can limit the displacement but may create high-frequency and

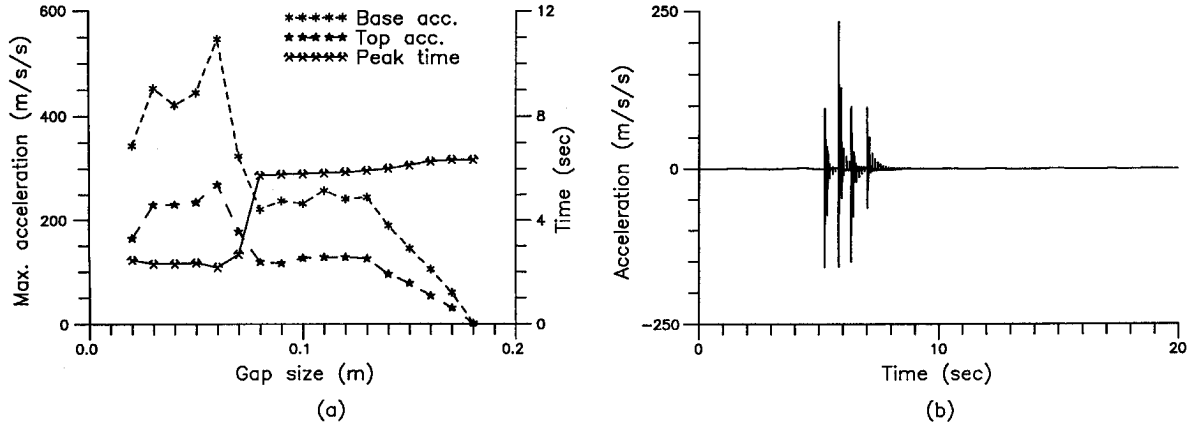

Figure 5. Response of elastic shear beam bumping against linear elastic stops: (a) variation of maximum acceleration with gap size; (b) base acceleration history for gap =0·10 m

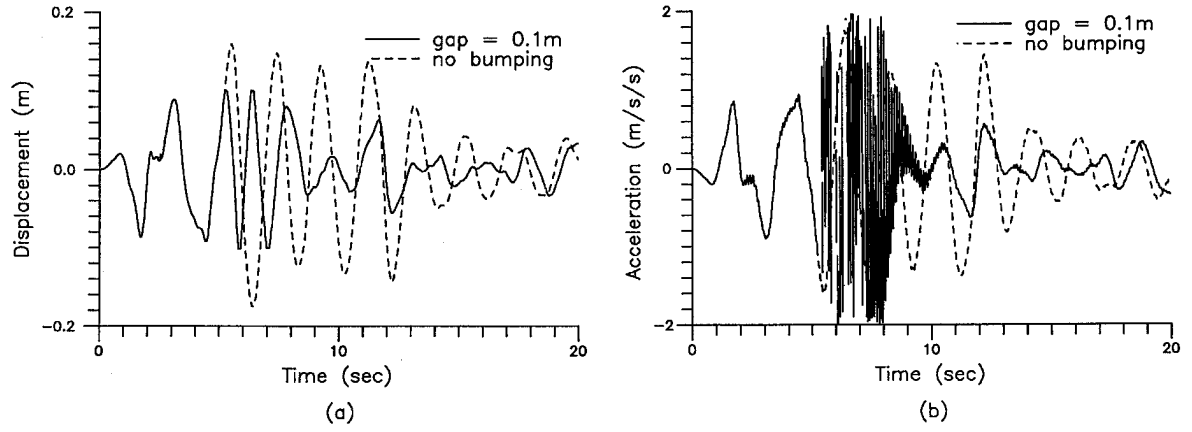

Figure 6. Base responses with and without bumping against linear elastic stops: (a) displacement; (b) acceleration

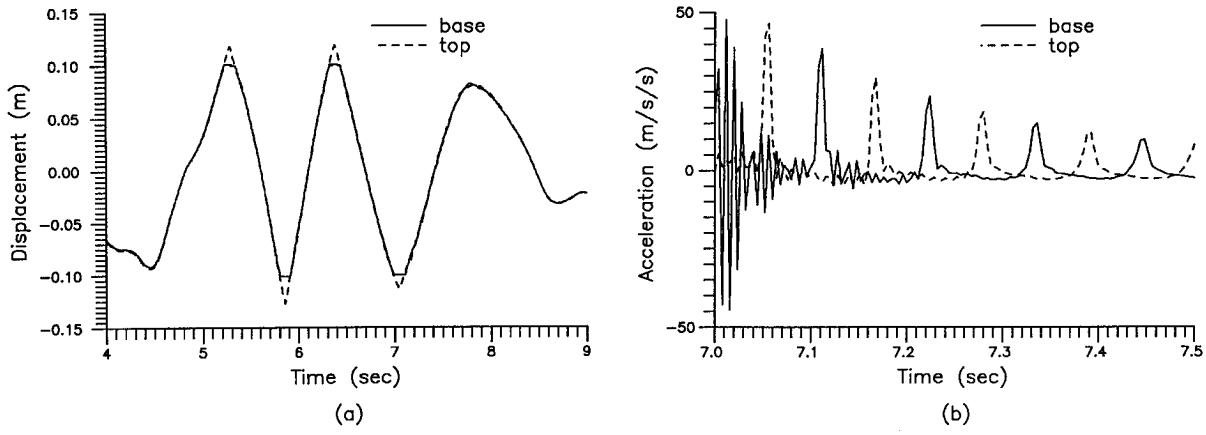

Figure 7. Responses at the top and base of shear beam bumping against linear elastic stops: (a) displacement; (b) acceleration

high-amplitude acceleration response. The high-frequency spikes induced by the bumping quickly decay and die out after the ninth second.

The responses at the top and the base of the shear beam during the bumping are compared in Figure 7. The displacement histories shown in Figure 7(a) are almost the same, except for that, during the shear beam contacting with the stops, the displacement history at the base is flat. However, the curve at the top is sharply varied because, when the motion of the base is constrained by the stops, the top of the shear beam can continue to deform. The acceleration histories at the base and the top after the fourth bumping which occurs at the seventh second are shown in Figure 7(b), which reveals the travelling speed of the stress wave created by the impact of the stop. The time interval between the two consecutive peaks at the base or at the top is 0·111 s which is the duration in which the stress wave travels back and forth in the shear beam. Restated, the wave velocity is 270 m/s, which is equal to the magnitude of $\sqrt{GA_s/\rho A}$. The amplitude of the impact wave gradually decays because of the damping in the shear beam.

Because the duration of the shear beam contacting with the stops is very short, increasing the stop damping has little effect on lowering the acceleration of the shear beam. Numerical results reveal that, if the stop damping is increased from zero to 66·4 kN s/m, the maximum acceleration changes from 233 to 241 m/s^2 at the base and from 127 to 126 m/s^2 at the top.

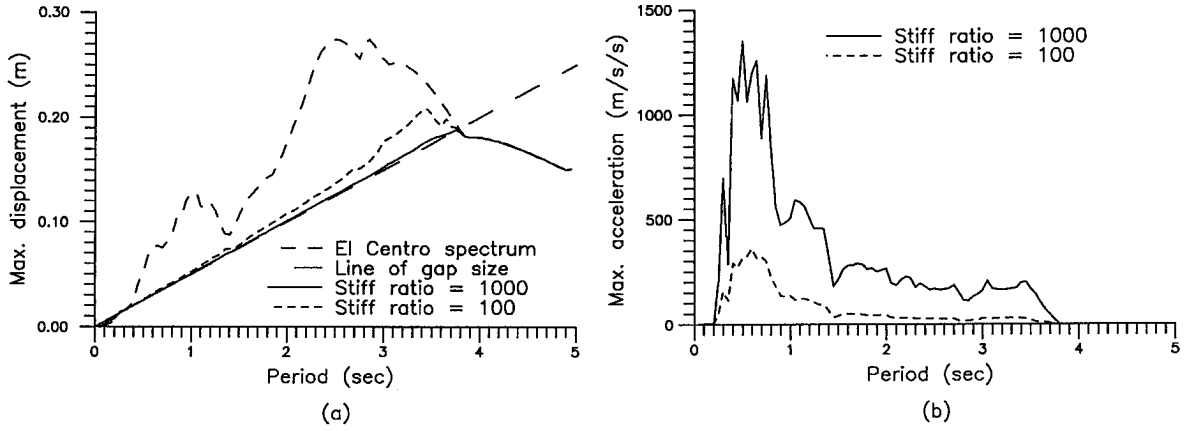

Figure 8. Variation of maximum base responses with periods: (a) displacement; (b) acceleration

The response spectra of general earthquakes have a common feature that there is nearly a constant velocity response in the range between approximately 0·3 to 2 Hz.[6] Since the natural frequencies for most of the base-isolated buildings are located in this range, the 'extreme' velocity spectrum, S_v, applied in base isolation can be regarded as a constant value. The minimum size of the isolation gap to prevent the isolated building from bumping becomes linearly varied with the period of the isolation system, T_b.

$$D = \frac{S_v}{\omega_b} = \frac{S_v T_b}{2\pi} \tag{21}$$

Figure 8(a) shows the displacement spectrum of the El Centro earthquake and the line of gap size calculated according to equation (21) with $S_v = 0{\cdot}314$ m/s. Bumping can occur at the natural periods where the displacement spectrum is higher than the line of gap size. A higher value of S_v has a shorter range of the natural period in which bumping can occur. The maximum base responses varied with the isolator period are plotted in Figure 8 for the stiffness ratios $R_k = 1000$ and $R_k = 100$, which indicates that smaller stop stiffness has higher displacement response but has lower acceleration response.

5. RESPONSE FOR NON-LINEARLY ELASTIC STOP

Because the large stiffness difference between the isolator and the stop, when the shear beam starts to make contact with the stop, the sudden change of the stiffness at the base of the shear beam creates the high acceleration response. The results shown in Figure 8(b) indicates that the high acceleration response may be reduced if the stop stiffness is gradually increased with increasing displacement. To verify this, the following non-linear force–displacement model of the stop is proposed:

$$f_S = k_1 bd \left(\frac{v_b - d}{bd} \right)^a \tag{22}$$

in which f_S is the spring force of the stop, v_b is the displacement at the base, d is the gap size, k_1 is the stiffness parameter, a and b are the two parameters to describe the non-linear model. The curves of equation (22) having the same b but different a are plotted in Figure 3(b). All curves intersect at the same point of $v_b = (1 + b)d$ and $f_S = b(k_1 d)$. Larger value of a implies a higher non-linearity. When $a = 1$, equation (22) becomes the linear stop defined in Figure 3(a) and $k_1 = k_s$. When $v_b/d < 1 + b$, larger a has smaller spring force, but after

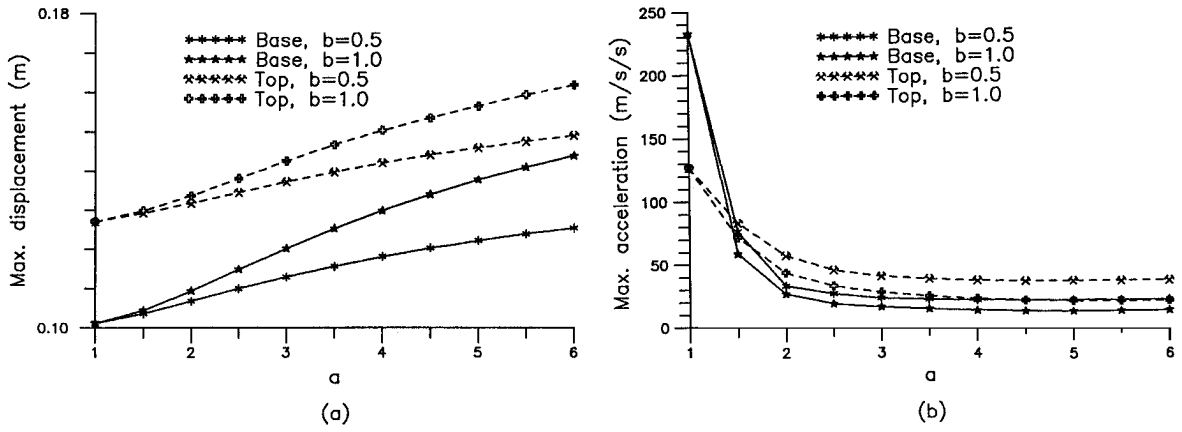

Figure 9. Maximum responses of shear beam bumping against non-linear elastic stops: (a) displacement; (b) acceleration

$v_b/d > 1 + b$, larger a becomes to have higher spring force. The tangential stiffness of equation (22) is

$$\frac{\partial f_S}{\partial v_b} = ak_1 \left(\frac{v_b - d}{bd} \right)^{a-1} \tag{23}$$

which indicates that the tangential stiffness at the intersecting point is ak_1.

The maximum responses of the shear beam model described in the last section and excited by the El Centro record are compared in Figure 9 for various non-linear stops, which indicates that increasing a or b can increase displacement response and decrease acceleration response. The stiffness of the linear isolator is $k_b = 210\,\text{kN/m}$ and the damping coefficient is $c_b = 6640\,\text{N s/m}$. All stops have the same gap size and stiffness parameter, $d = 0 \cdot 10\,\text{m}$ and $k_1/k_b = 1000$. Compared with the response of the linear stop ($a = 1$), Figure 9(b) shows that the non-linear stops of $a \geqslant 2$ can significantly reduce the acceleration response. When $a > 4$, however, increasing the value of a can only increase the displacement and has little effect on reducing the acceleration. The optimum a value ranges between 2 and 4. When $a = 1$, the acceleration response at the base is higher than that at the top. As the value of a increases, however, the acceleration at the top becomes higher than that at the base. Restated, a value is more efficient at reducing the base acceleration than the top acceleration.

For non-linear stops, there is a transition zone of deformation in which the stiffness is smaller than the linear stiffness k_1, so that the deformation of the non-linear stops is always larger than that of the linear stop, $a = 1$, if using the same d value . The transition zone can be defined by the equivalent gap size, d_e, which is the displacement v_b at which the tangential stiffness is equal to k_1 and can be derived from equation (23) as

$$d_e = \left(1 + \frac{b}{a^{1/(a-1)}} \right) d \tag{24}$$

For the linear stop, the equivalent gap size is the actual gap size, i.e., $d_e = d$. For the non-linear stop, each set of a and b values corresponds with an equivalent gap size. Studying the effect of the non-linear stop requires making a comparison of the responses of the non-linear stop with the linear stop at the same equivalent gap size. The maximum base accelerations of the non-linear stops in Figure 9(b) are replotted in Figure 10(a) according to the equivalent gap size, which reveals that, under the same equivalent gap size, the non-linear stop has a smaller maximum acceleration response than the linear stop. Since the optimum a value is between 2 and 4, the b value can be calculated from equation (24) when the equivalent gap size is determined.

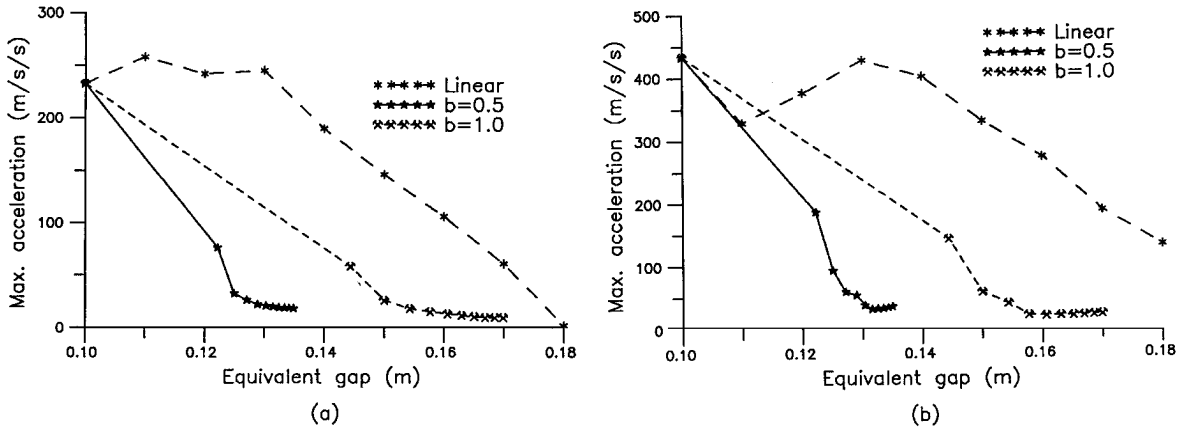

Figure 10. Variation of maximum base acceleration with equivalent gap sizes of linear and non-linear elastic stops: (a) linear isolator; (b) bilinear isolator

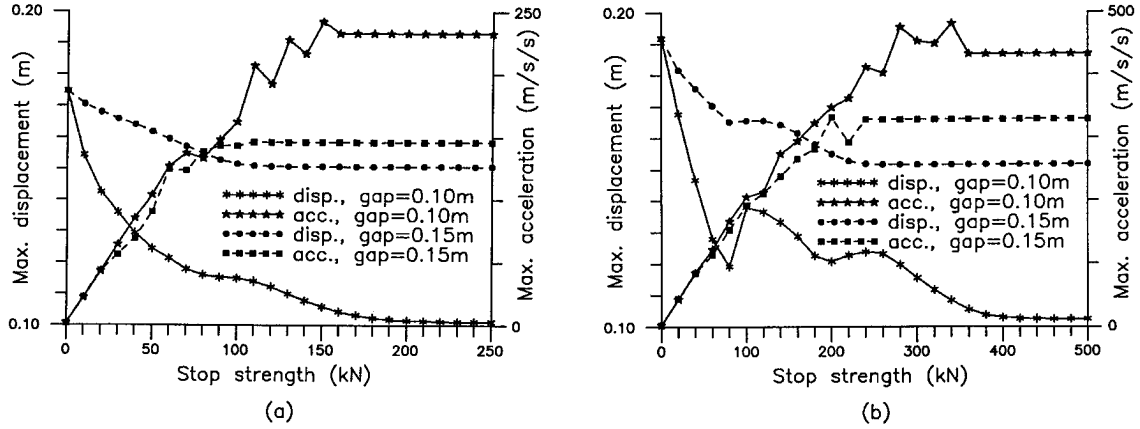

Figure 11. Variation of maximum base response with stop strength of inelastic stops: (a) linear isolator; (b) bilinear isolator

6. RESPONSE FOR INELASTIC STOP

The high-acceleration response in the analysis of the linearly elastic stops indicates that the stops are subjected to the extremely large impulsive force during the bumping, which can cause the stops to be in the inelastic stage. To capture the more realistic behaviour of bumping, the stop is modelled as an elastoplastic spring of which the force–displacement relation is shown in Figure 3(c) where k_s is the elastic stiffness, f_p is the stop strength and d is the initial gap size. The yielding of the stop creates the permanent set and increases the gap size.

The properties of the shear beam and the isolator utilized in the analysis of the inelastic stop are the same as those utilized in the last section. The elastic stiffness of the inelastic stop is $k_s = 210\,\mathrm{MN/m}$. The responses of the shear beam excited by the El Centro record are calculated for two different gap sizes, $d = 0{\cdot}10$ m and $d = 0{\cdot}15$ m, and stop strengths varied from 0 to 250 kN. The maximum displacements and accelerations at the base of the shear beam are plotted in Figure 11(a). This figure shows that, for small stop strength, the maximum acceleration increases and the maximum displacement decreases with increasing stop strength. When the stop strength increases to a certain value, the stop does not yield and the responses are the same as those of the linearly elastic stop. However, before reaching this value, there is a range of stop strength where

the variation of the maximum acceleration is small. For the example of the 0·1 m gap size, the maximum acceleration increases from 1·75 to 227 m/s^2 when the stop strength increases from 0 to 130 kN. But from 130 to 230 kN, the maximum acceleration only increases from 227 to 232 m/s^2. When the stop strength is greater than 230 kN, the stop does not yield and the maximum acceleration remains at 232 m/s^2. For the low stop strength, the yielding of stop can dissipate energy and enlarge the gap size, so that the maximum acceleration response is clearly smaller than the response of the elastic stop. For the high stop strength, more rebound energy is stored in the elastic strain energy of the stop, so that the plastic deformation is small and the reduction of the maximum acceleration is little.

7. RESPONSE OF BILINEAR ISOLATOR

Some types of isolation system have bilinear force–displacement relation as shown in Figure 4(b) in which k_e is the elastic stiffness, k_p is the yield stiffness and f_y is the yield force. The bilinear isolator used in the numerical study has $k_p = 210$ kN/m and $k_e/k_p = 10$. The yield force is $f_y = 10{\cdot}5$ kN which is approximately 5 per cent of the total weight. The hysteretic damping of the bilinear isolator can dissipate a lot of energy. Its response must be smaller than that of the linear isolator, so that the input acceleration uses the El Centro earthquake multiplied by a scale factor of two. Using of the same model of the shear beam, numerical results shown in Figure 10(b) is the maximum base acceleration bumping against the elastic stops, which reveals that the non-linearly elastic stop can reduce the acceleration response of the bilinear isolators.

The maximum responses of the bilinear isolator bumping against the inelastic stops are plotted in Figure 11(b), which indicates that the bumping of the bilinear isolator possesses some characteristics similar to the bumping of the linear isolator shown in Figure 11(a). In the case of the 0·1 m gap size, when the stop strength is greater than 460 kN, the stop does not yield and the maximum acceleration remains at 433 m/s^2. However, in the range of stop strength between 280 and 340 kN, the maximum accelerations are higher than 433 m/s^2. In other words, for the high stop strength, the maximum acceleration response of the inelastic stops may be larger than that of the elastic stops.

8. INELASTIC SUPERSTRUCTURAL RESPONSE

During extreme earthquake events, the superstructure may experience inelastic response. Since the formulation presented in the second section is unable to handle local yielding of shear beam, the non-linear finite element method is applied to analyse the inelastic response of shear beam. After discretized by the shear-beam elements, the model has the same governing equilibrium equation as equation (14) but does not possess the simple form like equation (17).

In the numerical study, the aforementioned shear beam is discretized into ten elements. The length of each element is 1·5 m. Unless further specified, the following parameters are used. The post-yield stiffness of the shear beam is equal to 0·5 per cent of the elastic stiffness. In the case of the linear isolator, the yield strength of the shear beam is 63 kN so that the yield displacement of the elements is 0·926 mm; the input acceleration uses the El Centro record multiplied by a scale factor of two. The linear isolator has $k_b = 210$ kN/m and $c_b = 6640$ N s/m. In the case of the bilinear isolator, the peak ground acceleration and the yield strength of the shear beam are the double of those used in the linear isolator. The properties of the bilinear isolator are the same as those defined in the last section. The stiffness of the linearly elastic stop is 210 MN/m. The elastic stiffness of the inelastic stop has the same value.

The numerical results show the bumping against the stops creates high acceleration only at the base of the shear beam. Because of the yielding of the lowest element, the impact wave does not propagate into the upper level of the shear beam so that the shear beam still has low acceleration response. The distributions of element ductility, defined as the maximum element deformation divided by the yield deformation of the element, along the shear beam are shown in Figure 12(a) for different stop stiffness, which reveals that variation of the stop

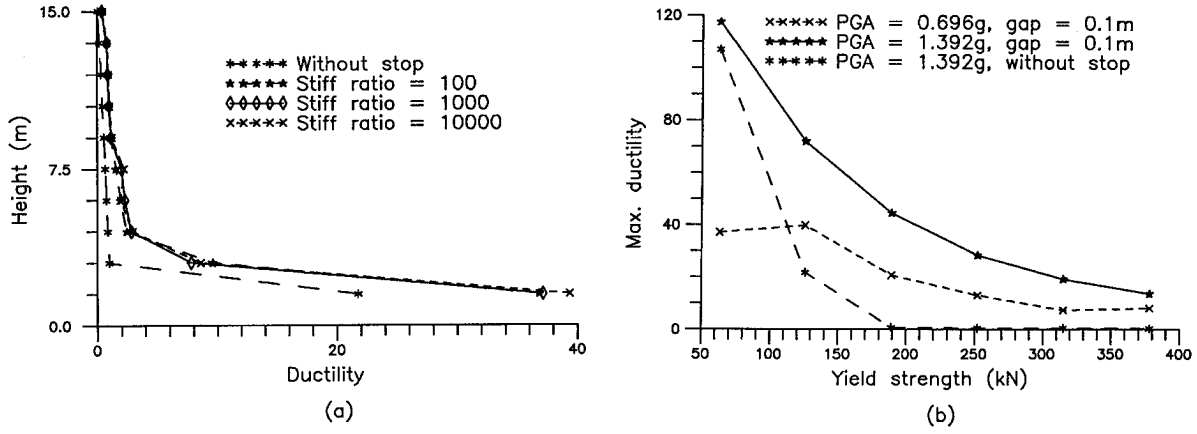

Figure 12. Inelastic response of shear beam with linear isolator bumping against linear elastic stops: (a) ductility distribution for different stop stiffness; (b) variation of maximum ductility with yield strength

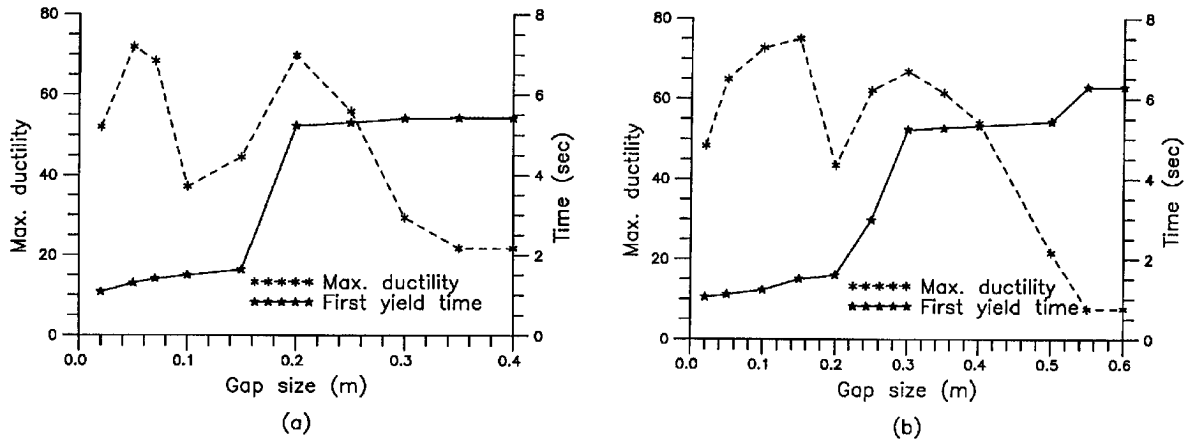

Figure 13. Variation of maximum ductility of inelastic shear beam with gap size of linear elastic stops: (a) linear isolator; (b) bilinear isolator

stiffness has little effect on the distribution of ductility demand. However, high stop stiffness still creates high acceleration response at the base of the shear beam.

The variations of the maximum ductility, occurred at the lowest element, with the yield strengths are shown in Figure 12(b) for the inputs of two different scales, which indicates that maximum ductility tends to decrease with increasing yield strength and increase with increasing peak ground acceleration. At the high yield strength where the shear beam did not yield if without stop, the impact force generated by the bumping against the stops leads towards the yielding of the shear beam.

The influence of the gap size of the linearly elastic stops on the maximum ductility is shown in Figure 13(a) for the linear isolator and in Figure 13(b) for the bilinear isolator. Also shown in these figure are the times when the shear beam starts to yield. The responses of the linear and the bilinear isolator possess the same characteristics; when the gap size increases, two peaks of the maximum ductility are observed, which corresponds to the different first yield times. This variation is similar to the acceleration response of the elastic shear beam shown in Figure 5(a).

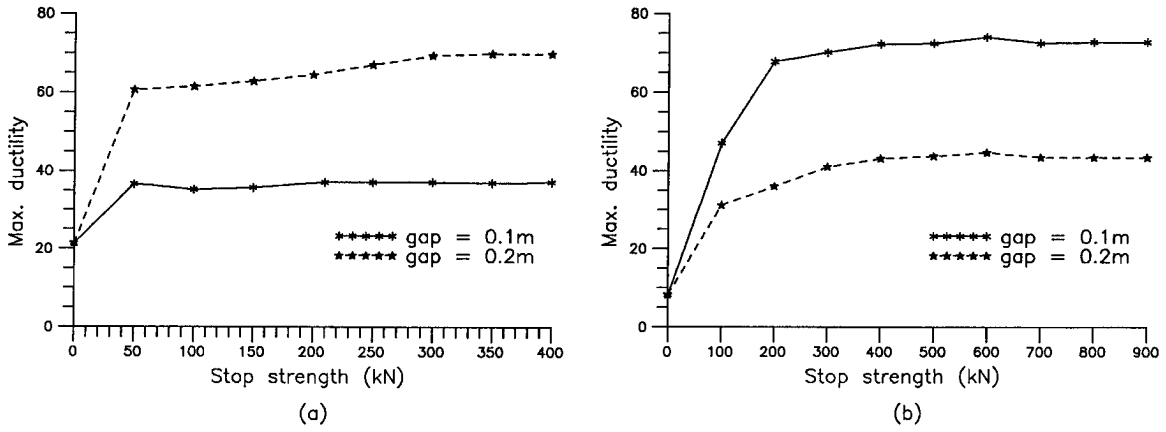

Figure 14. Variation of maximum ductility of inelastic shear beam with stop strength of inelastic stops: (a) linear isolator; (b) bilinear isolator

The influence of the stop strength of the inelastic stop on the maximum ductility is shown in Figure 14(a) for the linear isolator and Figure 14(b) for the bilinear isolator. These figures show that the maximum ductility is reduced only for the lower stop strength. For the higher stop strength, the maximum ductility of the shear beam bumping against the inelastic stop is almost the same as that against the elastic stop shown in Figure 13.

9. CONCLUSIONS

The influence of stop stiffness, gap size and stop strength on the seismic response of base-isolated shear beams bumping against stops has been presented. Both of the elastic and inelastic responses of base-isolated shear beams are studied. Because of the large difference between the isolator stiffness and the stop stiffness, when the base-isolated shear beam bumps against the stops, the sudden change of the stiffness at the base of the shear beam creates impact waves.

If the shear beam remains elastic, the impact waves can travel along the beam and induce the extremely high acceleration response in the shear beam. Numerical results indicate that adding viscous damping to the stops has an insignificant effect on reducing the beam acceleration. However, the acceleration response can be dramatically reduced, if the stops possess the non-linearly elastic behaviour of which the stiffness increases with increasing deformation. In the case of the low stop strength, the yielding of stop can dissipate energy and reduce the acceleration response, but pays the price of increasing the displacement. For the high stop strength, the reduction of acceleration is minor and the response of the inelastic stop is almost the same as that of the elastic stop.

If the shear beam yields during excitation, the impact waves cannot propagate through the shear beam and only the base of the shear beam subjects to high acceleration. Changing the stop stiffness or stop strength does not affect the distribution of ductility demand along the shear beam.

Since only horizontal degrees of freedom are considered, this study is applicable only to short base-isolated structures where uplift is not an issue. A tall or slender base-isolated structure will undergo a rocking mode when impacted against restraints and further study is required.

ACKNOWLEDGEMENTS

The author would like to thank the National Science Council, Republic of China, for its partial financial support of this manuscript under Contract No. NSC 82-0410-E011-053.

REFERENCES

1. J. P. Moehle (ed.), 'Preliminary report on the seismological and engineering aspects of the January 17, 1994, Northridge earthquake', *Report No. UCB/EERC-94/01*, Earthquake Engineering Research Center, University of California, Berkeley, CA, 1994.
2. V. Zayas, A. Low, L. Bozzo and S. Mahin, 'Feasibility and performance studies on improving the earthquake resistance of new and existing buildings using the friction pendulum system', *Report No. UCB/EERC-89/09*, Earthquake Engineering Research Center, University of California, Berkeley, CA, 1989.
3. J. M. Kelly, I. G. Buckle and H.-C. Tsai, 'Earthquake simulator testing of a base-isolated bridge deck', *Report No. UCB/EERC-85/09*, Earthquake Engineering Research Center, University of California, Berkeley, CA, 1986.
4. J. M. Kelly, K. E. Beucke and M. S. Skinner, 'Experimental testing of a friction damped aseismic base isolation system with fail-safe characteristics', *Report No. UCB/EERC-80/18*, Earthquake Engineering Research Center, University of California, Berkeley, CA, 1980.
5. K. J. Bathe, *Finite Element Procedures in Engineering Analysis*, Prentice-Hall, Englewood Cliffs, NJ, 1982.
6. A. K. Chopra, *Dynamics of Structures*, Prentice-Hall, Englewood Cliffs, NJ, 1995.

